Electroacoustics modeling of piezoelectric welders for Ultrasonic Additive Manufacturing processes

Adam Hehr[a] and Marcelo J. Dapino[a]

[a]NSF I/UCRC on Smart Vehicle Concepts, Department of Mechanical and Aerospace Engineering, The Ohio State University, 201 W 19th Ave. Columbus, Ohio 43210

ABSTRACT

Ultrasonic additive manufacturing (UAM) is a recent 3D metal printing technology which utilizes ultrasonic vibrations from high power piezoelectric transducers to additively weld similar and dissimilar metal foils. CNC machining is used intermittent of welding to create internal channels, embed temperature sensitive components, sensors, and materials, and for net shaping parts. Structural dynamics of the welder and work piece influence the performance of the welder and part quality. To understand the impact of structural dynamics on UAM, a linear time-invariant model is used to relate system shear force and electric current inputs to the system outputs of welder velocity and voltage. Frequency response measurements are combined with in-situ operating measurements of the welder to identify model parameters and to verify model assumptions. The proposed LTI model can enhance process consistency, performance, and guide the development of improved quality monitoring and control strategies.

Keywords: ultrasonic additive manufacturing (UAM), additive manufacturing, LTI modeling, frequency response function (FRF), piezoelectric, ultrasonic welding

1. INTRODUCTION

Ultrasonic additive manufacturing (UAM) or ultrasonic consolidation is a continuous solid-state additive manufacturing process through which thin foils of similar or dissimilar metals are ultrasonically welded together in a layer by layer process to form gapless, 3D metal parts.[1,2] The process begins by bringing a tool piece called the sonotrode or horn into contact with a metallic foil under a controlled pressure or normal load. Then, the sonotrode is actuated with one or two high power piezoelectric transducers to scrub the metallic foil to the pre-deposited metal beneath. The circular design of the sonotrode allows it to rotate at a prescribed linear speed simultaneous to welding. Periodic CNC machining is utilized intermittent of welding to create complex internal features, embed objects into the structure, and for net shaping welded components. The sonotrode and piezoelectric transducers are designed to resonate longitudinally near 20 kHz, so the welder resonance is near 20 kHz too. Recently, the process has been improved upon by actuating the sonotrode with two high power transducers.[3] This dual actuation increases the delivered weld power from 1 kW to 9 kW. As a result of the power increase, weld quality has greatly improved.[4] Photos of a 9 kW UAM system are shown in Figure 1.

The key mechanisms for ultrasonic metal welding include oxide fracture under pressure and plastic deformation of surface asperities through shear.[5–7] Oxide dispersal allows nascent metal surfaces to come into contact and form metallic bonds while surface asperity deformation promotes dynamic recrystallization of the interface microstructure.[8–11] The result is a narrow weld region on the order of 10-20 μm in size and bulk temperatures far below metallic melting temperatures.[12] Consequently, dissimilar metals can be welded together with minimal intermetallic formation,[13–17] metallurgical changes are minimized and highly localized to the interface region, and temperature sensitive metals or components can be combined or built into metal structures.[18–22] Examples of where UAM has been utilized to join dissimilar metals and integrate temperature sensitive components into metallic structures are shown in Figure 2.

Further author information: (Send correspondence to M.J. Dapino)
M.J.D.: E-mail: dapino.1@osu.edu, Telephone: 1 614 688 3689
A.H.: E-mail: hehr.7@osu.edu

Industrial and Commercial Applications of Smart Structures Technologies 2016,
edited by Steven F. Griffin, Proc. of SPIE Vol. 9801, 98010F · © 2016 SPIE
CCC code: 0277-786X/16/$18 · doi: 10.1117/12.2219570

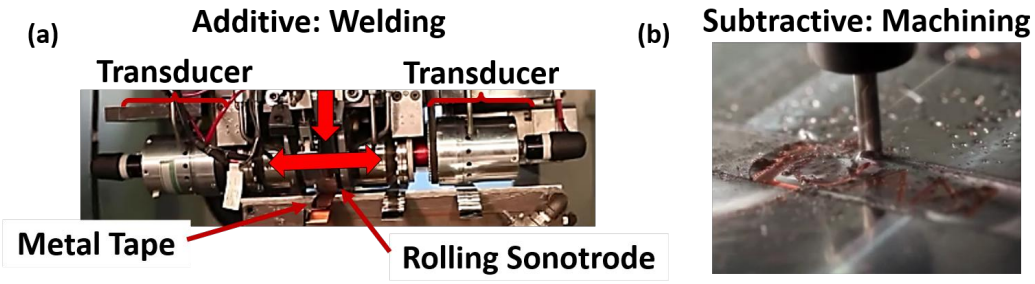

Figure 1. SonicLayer 4000 ultrasonic additive manufacturing system: (a) the welder is used to additively join foils together; (b) the subtractive CNC stage is used for introducing complex internal features and for trimming components. The ultrasonic transducers are fabricated by Dukane and are each rated to 4.8 kW. The down arrow represents the applied down force during welding while the side-side arrow represents the vibratory scrubbing action.

The focus of this paper is to describe UAM system dynamics with a linear time-invariant (LTI) model of the welding assembly which explicitly specifies welder shear force and electric current as system inputs. The outputs of the model are welder velocity and electric voltage. Conventional LTI models for ultrasonic systems lump the influence of shear force or load into the motional feedback of the entire system for control purposes,[23] i.e., Van Dyke system representation.[24] Because the focus of the paper is to describe the system dynamics of the welder, i.e., sonotrode and transducers, it is required to explicitly express shear force as a system input. This alternative LTI model can be used for improved control strategies and energy transfer analysis for UAM.

The paper begins by describing how the UAM process is controlled and how the control strategy relates to welder performance. Then, the system is described in terms of impedance relations in order to convey the proposed LTI model. Experimental frequency response functions (FRFs) of the welding assembly are then characterized using these impedance relations and compared to the LTI model. In-situ measurements of the welder operating under no load were then taken to evaluate welder performance as a function of amplitude level. These measurements were used to verify and to find the LTI model parameters for the mechanical mobility representation of the welder. Lastly, shear force and welder efficiency are estimated utilizing the LTI model and in-situ measurements.

2. UAM CONTROL BACKGROUND

UAM has been utilized for about a decade, yet the process uses ultrasonic metal welding control strategies developed long ago. Ultrasonic metal welding control strategies are designed for single metal joints. In UAM, many joints are made throughout the UAM process and the build geometry changes throughout component construction. Consequently, unwanted resonances can occur[25,26] and the amount of deformation at the weld interface changes as the build becomes more compliant.[27,28] Due to less deformation occurring at the weld interface, the part quality degrades. A control strategy unique to UAM is needed to avoid or minimize undesired structural dynamics and to maintain weld quality throughout component construction. Such a control strategy can be developed with a reliable system level model of the UAM process.

Control dynamics of the UAM process change when welding vs. actuating the sonotrode without load (no welding), see Figure 3. In particular, the peak velocity or scrubbing motion decreases 10% (Figure 3(a)), the frequency of the welder increases 75 Hz (Figure 3(b)), and the electric power draw of the piezoelectric transducers increases an order of magnitude, see Figure 3(c). A customized ultrasonic generator for the UAM process is responsible for the control dynamics observed in Figure 3. The generator uses two closed loop controllers which work simultaneously. The first controller uses a phase lock loop (PLL) algorithm to track system resonance during welding by minimizing the phase angle between the applied voltage and current.[29,30] This PLL algorithm is the reason for the frequency shift seen in Figure 3(b). System resonance can change when welding due to added mass, stiffness, and heat generation from the load.[30–32] An upward frequency shift such as the one seen in Figure 3(b) can only occur from an increase in stiffness. This stiffness increase originates in the psuedo-stick condition that occurs during welding.[33]

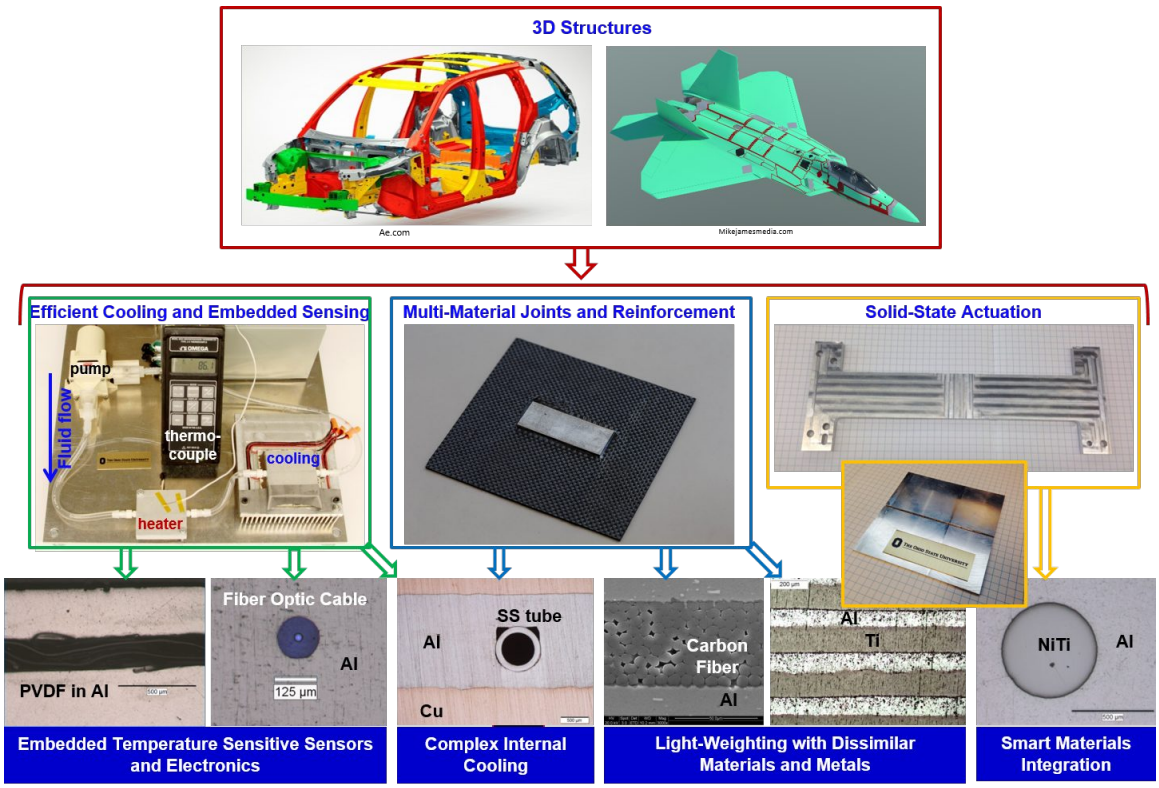

Figure 2. Potential UAM applications. The low formation temperature of UAM enables joining dissimilar metals (without the formation of brittle intermetallics) and the integration of temperature sensitive components, smart materials, cooling channels, organic polymers, and electronics into metal matrices.

The second controller works to maintain welder amplitude as the part is built, which under open loop conditions would result in a decrease in amplitude. Welder amplitude in UAM is maintained by controlling voltage to be constant. Voltage is controlled by varying the current to maintain a set-point value for a given amplitude setting.[34] Further details on voltage control are provided in Section 5. Ultrasonic systems can also be controlled using electric current in a similar manner.[23,30]

In order to accurately track the resonance of the system for both the PLL algorithm and amplitude control, the mechanical motion of the welder needs to be measured. The most common way of measuring mechanical motion is with the use of motional feedback methods. Motional feedback works by adding a reactive element in series or in parallel with the transducer to balance out its electrical impedance or admittance.[23,30–32] For piezoelectric systems, this reactive element is an inductor. By balancing out the electrical impedance of the transducer, the motional impedance or motion of the transducer can be indirectly measured with applied current and voltage to the transducer. There are many different circuits utilized to implement motional feedback control techniques.[23,32] The ultrasonic generator used on UAM systems utilizes such a motional feedback method for resonance tracking and amplitude control. Because amplitude is not measured directly in UAM, a decrease in vibration can occur if the reactive inductance element does not sufficiently isolate the motional impedance of the transducer or if significant compliance exists in the sonotrode,[33] see Figure 3(a). Lastly, because voltage is controlled to be constant by increasing electric current during welding, the average electric power draw increases substantially to maintain welder motion, see Figure 3(c).

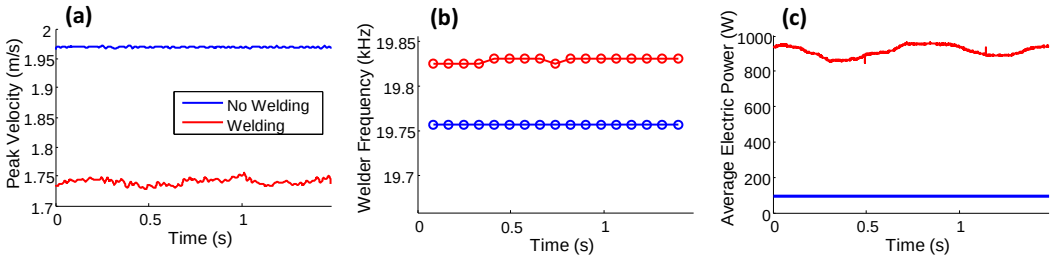

Figure 3. UAM system dynamics and control when not welding, i.e., exciting welder in air without load, and welding Al 6061 foil: (a) peak sonotrode or welder velocity; (b) excitation frequency; (c) average electric power draw from one of the ultrasonic transducers. Data was collected using the welding process variables of 32.5 μm peak-peak prescribed welder vibration, a down force of 5000 N, and a rolling speed of 5 m/min (200 in/min). Data was sampled at 50 kHz and processed with a block size of 8192 points, welder vibration was measured with a non-contact laser vibrometer, welder frequency was obtained using a short time windowed FFT, and power draw was sampled directly from the ultrasonic generator.

3. TIME-INVARIANT LINEAR MODEL OF UAM PROCESS

To describe the system dynamics of the welder for all frequencies (ω), the following LTI system model with voltage-force as across variables and velocity-current as flow variables for the system can be written,

$$\begin{pmatrix} i(j\omega) \\ \dot{\delta}(j\omega) \end{pmatrix} = \begin{bmatrix} H_e(j\omega) & H_{me}(j\omega) \\ H_{em}(j\omega) & H_m(j\omega) \end{bmatrix} \begin{pmatrix} V(j\omega) \\ F_s(j\omega) \end{pmatrix}, \tag{1}$$

where H_e is the FRF between applied voltage (V) and electric current (i), H_{me} is the FRF between opposing shear force during welding (F_s) and current, H_{em} is the FRF between applied voltage and velocity of the sonotrode ($\dot{\delta}$), and H_m is the FRF between shear force and velocity. Due to the system being piezoelectric, the system follows the law of reciprocity.[24,35] As a result, H_{me} and H_{em} are equal in magnitude and phase. This LTI model with force as the across variable and velocity as the flow variable is proposed initially due to piezoelectric systems conventionally using this form,[23,24,35] and because the system is feasible to characterize in this form. An equivalent LTI model of the system using velocity as the across variable and force as the flow variable will be presented toward the end of this section because the motional feedback controller utilizes this relationship. The equivalent form is derived using the principle of duality.[35] Both LTI models can be used to describe the system behavior because the system behaves in a steady manner during welding operations, as evidenced by the stable welding traces in Figure 3. The system exhibits a small amount of variation when welding because the PLL algorithm moves the voltage excitation frequency. This small frequency shift in the PLL controller may originate from variations in the UAM build compliance and shear force character during welding.

To understand the relation between system physics and the FRF terms, equivalent circuit analysis can be used to derive closed form FRF expressions near resonance. To model the electro-mechanical coupling of the piezoelectric transducers, an ideal transformer can be utilized.[24,36] A schematic of the welding assembly along with its corresponding equivalent circuits are shown in Figure 4. The equivalent circuit analysis is conducted assuming that the welding assembly is geometrically symmetric in shape and properties and that the two transducers operate out of phase, i.e., push-pull configuration. The system can be assumed to be geometrically symmetric because the sonotrode is precision machined, and the two transducers used to drive the sonotrode exhibit near identical response.[37] Because the system is geometrically symmetric and the transducers are operated out of phase, the transducers can be lumped together as a single transducer driving the sonotrode. The out of phase actuation of the welder is shown in Figure 4(a) with opposing voltage directions. The sonotrode in Figure 4(b) is modeled as a black box 2-port electrical network because (i) the transducers actuate the sonotrode at a different location than the shear force, and (ii) the influence of sonotrode on system performance is not considered in this paper. Because sonotrode design is not an aspect of this paper, Figure 4(b) can be simplified by lumping the transducer and sonotrode dynamics together, see Figure 4(c). These two devices can be lumped together

because both the transducers and sonotrode are designed to resonate at the driving frequency of 20 kHz. The equivalent circuit seen in Figure 4(c) is the Mason circuit representation for piezoelectric devices.[24]

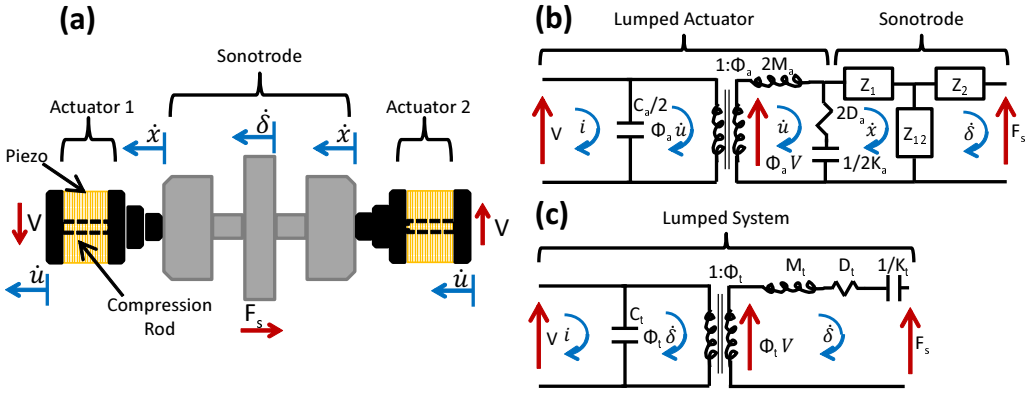

Figure 4. UAM weld assembly analysis: (a) schematic of assembly with components, voltages, forces, and degrees of freedom detailed; (b) equivalent circuit of weld assembly with transducers and sonotrode modeled separately; (c) simplified equivalent circuit of weld assembly by lumping the transducers and sonotrode dynamics together.

System FRFs can be derived from the equivalent circuit shown in Figure 4(c) by shorting out one input at a time and relating system outputs,[24]

$$H_e = \frac{i}{V} = j\omega C_t + \frac{\Phi_t^2}{j\omega M_t + D_t + \frac{K_t}{j\omega}}, \tag{2}$$

$$H_{em} = \frac{\dot{\delta}}{V} = \frac{\Phi_t}{j\omega M_t + D_t + \frac{K_t}{j\omega}}, \tag{3}$$

$$H_m = \frac{\dot{\delta}}{F_s} = \frac{1}{j\omega M_t + D_t + \frac{K_t}{j\omega}}, \tag{4}$$

where C_t is the capacitance of the transducers, Φ_t is the electro-mechanical transformer coefficient or turns ratio of the system, M_t is the effective mass of the system, K_t is the effective stiffness of the system, and D_t is the effective damping of the system.

Using the principle of duality, the equivalent circuit in Figure 4(c) can be redrawn using velocity as the across variable and shear force as the flow variable, see Figure 5. This system form is called the mechanical mobility equivalent circuit of the system,[35] and the welder utilizes it for control purposes. As mentioned earlier, motional feedback or purely electric signal feedback is utilized by the ultrasonic generator to maintain welder amplitude or velocity during welding. Motional feedback works by inserting an external inductor in series with the capacitive element of the transducer, see Figure 5(a). If the inductor impedance is chosen to be equal to the capacitor impedance at resonance, the electrical impedance of the transducer is balanced-out or removed from the circuit, see Figure 5(b). By removing the capacitance of the transducer near resonance, the motional impedance of the transducer can be isolated for control purposes, hence the name motional feedback. Welder velocity is directly related to applied voltage too and can be used for amplitude control purposes.

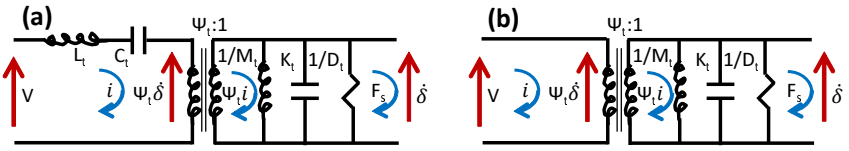

Figure 5. Equivalent circuit for welder operation: (a) mobility form of system with added inductance to balance-out transducer capacitance; (b) simplified mobility form of system without electrical influences from transducer, i.e. motional feedback form.

An equivalent LTI model using current and shear force as inputs and velocity and voltage as outputs can then be written,

$$\begin{pmatrix} V(j\omega) \\ \dot{\delta}(j\omega) \end{pmatrix} = \begin{bmatrix} H_e^*(j\omega) & H_{me}^*(j\omega) \\ H_{em}^*(j\omega) & H_m^*(j\omega) \end{bmatrix} \begin{pmatrix} i(j\omega) \\ F_s(j\omega) \end{pmatrix}, \tag{5}$$

where H_e^* is the FRF between electric current and voltage (V), H_{me}^* is the FRF between shear force and voltage, H_{em}^* is the FRF between electric current and welder velocity, and H_m^* is the FRF between shear force and velocity. H_{me}^* and H_{em}^* are equal in magnitude and phase like the other LTI model of the welder. These FRFs can written in terms of lumped system parameters and assuming that the electrical impedance of the transducer is suppressed,

$$H_e^* = \frac{V}{i} = \frac{\Psi_t^2}{j\omega M_t + D_t + \frac{K_t}{j\omega}}, \tag{6}$$

$$H_{em}^* = \frac{\dot{\delta}}{i} = \frac{\Psi_t}{j\omega M_t + D_t + \frac{K_t}{j\omega}}, \tag{7}$$

$$H_m^* = \frac{\dot{\delta}}{F_s} = \frac{1}{j\omega M_t + D_t + \frac{K_t}{j\omega}}, \tag{8}$$

where Ψ_t is the electro-mechanical transformer coefficient of this equivalent form. The other lumped paramters are assumed to not be dependent on the particular equivalent circuit form because they influence the system resonance and system resonance is nearly identical between the two forms. To show that the presented lumped system models are valid, the dynamics of the welding assembly are investigated in more detail with the use of experimental FRF measurements and characterization techniques in the next two sections.

It can be assumed that the shear force and applied current in (5) are out of phase at the 20 kHz driving frequency (ω_o) because shear force opposes welder vibration directly. This out of phase shear force can be expressed with a minus sign,

$$\dot{\delta}(j\omega_o) = H_{em}^*(j\omega_o) i(j\omega_o) - H_m^*(j\omega_o) F_s(j\omega_o). \tag{9}$$

Similarly for voltage,

$$V(j\omega_o) = H_e^*(j\omega_o) i(j\omega_o) - H_{me}^*(j\omega_o) F_s(j\omega_o). \tag{10}$$

Relations (9) and (10) where derived with the assumption that the system dynamics at resonance can be described with harmonic excitation. Section 6 will show that this single tone assumption is valid and will utilize the expression for welder velocity (9) to back calculate welder shear force.

4. FREQUENCY RESPONSE FUNCTION ESTIMATION

The welding assembly was characterized inside the UAM machine during FRF estimation to emulate operating boundary conditions. To apply a controlled voltage and measure current across the piezoelectric transducers, an AE Techron LVC 5050 was utilized. A Polytec PSV-400 Doppler laser vibrometer was used to measure sonotrode motion in a non-contact manner. The ability to measure welder vibration in a non-contact way is important because any added mass and geometry will adversely influence the tuned resonance behavior of the system. A high frequency modal hammer (PCB 086C30) was used to input a known force impulse into the sonotrode. A modal hammer was utilized because mass loading on the structure would be minimized compared to piezo reaction mass excitation. Lastly, a Data Physics QUATTRO Dynamic Signal Analyzer was used to estimate H_1 FRFs. A characterization schematic is shown in Figure 6.

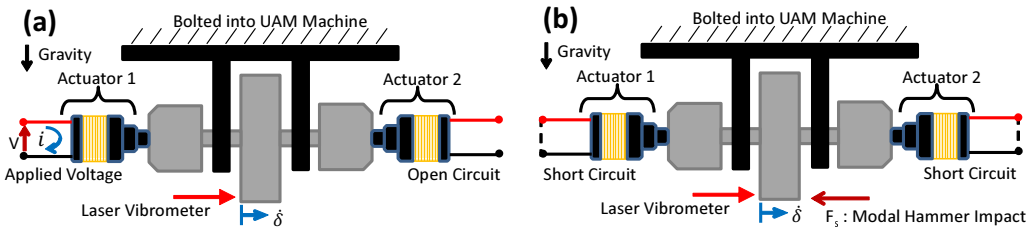

Figure 6. Conditions for assembly FRF measurements: (a) H_e and H_{em} measurements by driving one transducer and leaving the other open; (b) H_m measurement by shorting both transducers with a low resistance wire.

To measure H_e and H_{em}, one transducer was used to excite the system while the other was put into an open circuit condition. This characterization approach is valid because the system is symmetric, which makes the test conditions equivalent to driving the system with two transducers. Also, the open circuit condition is required to allow energy storage over the capacitor and to prohibit current flow out of the passive transducer. Because the resonance of the welder is lightly damped, swept sine excitation was utilized around the 20 kHz resonance of the system. Frequency spacing during the sweep was 0.5 Hz and measurements were taken until a minimum coherence value of 0.99 was reached for the frequencies of concern. To measure H_m, both transducers were short circuited with low resistance stranded wire while the modal hammer was used to excite the sonotrode. The transducers were short circuited so that energy would not be stored within the capacitive element of the transducers. FRF estimation utilized 10 hammer impacts for averaging and an exponential processing window to minimize leakage. Frequency resolution during H_m estimation was near 2.4 Hz, so measuring the peak FRF value was difficult.

The Mason circuit model of the welder is compared to experimental FRFs in Figure 7. The Mason circuit model was found using the measured FRF forms discussed earlier and with procedures given for an ideal Mason circuit.[24] The H_e FRF was used to estimate the capacitance, mass, stiffness, and damping of the transducers. The electro-mechanical transformer coefficient is found via the ratio of the mobility loop diameters of H_{em} and H_e. As seen in the Figure, the fit shows good correlation in magnitude with some error in phase. Phase error is believed to originate in the linear amplifier used to make the voltage and current measurements because 20 kHz is near the operating limit of the device. Consequently, phase error on the order of 15 degrees is possible.[38] Lumped model parameters for this fit are listed in Table 1.

Model Variable	Value
C_t (nF)	203.21
M_t (kg)	1.98
K_t (GN/m)	30.49
D_t (Ns/m)	82.05
Φ_t (N/V)	1.54

Table 1. Lumped parameter values for simplified equivalent circuit fit of welding assembly dynamics.

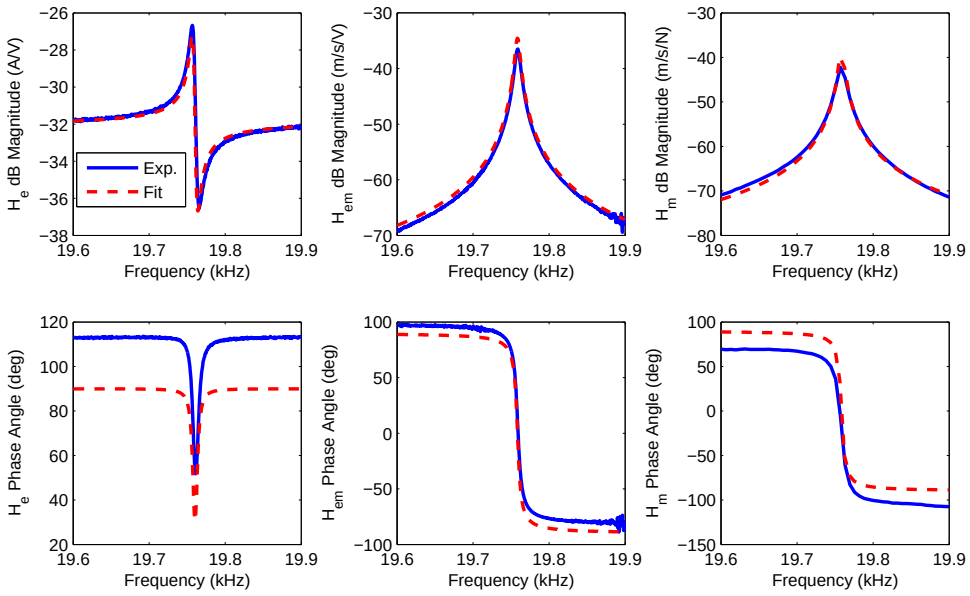

Figure 7. System FRF comparison between measurement and model.

5. WELDER OPERATION MEASUREMENTS

Because the measured system FRFs agree well with the Mason circuit shown in Figure 4, it can be inferred that the mechanical mobility representation of the welder shown in Figure 5 is also valid. To characterize this mechanical mobility representation of the welder, velocity, voltage, and average electric power measurements were made on the welder while it was operating without load. These three variables were evaluated at different amplitude settings of the ultrasonic generator. To measure welder velocity, the noncontact laser vibrometer was utilized. A Tektronix P6015A voltage probe was used with an Agilent 54622A oscilloscope to measure RMS voltage and P-P voltage of the welder. Power was measured by using the analog output channel on the ultrasonic generator.

To obtain accurate estimates for system voltage and power, the welder was driven with one transducer while the other was left in the open circuit condition. By driving the system with one transducer, the ultrasonic generator doubles the applied current to achieve the same voltage and welder velocity outputs.[37] Because current doubles and the voltage is constant, the power also doubles. Peak welder velocity and average electric power draw for the amplitude levels of 40, 50, 60, 70, and 80% are shown in Figure 8(a) while peak voltage is shown in Figure 8(b). It was found that the measured applied voltage was very similar to a sine wave, so the voltage in Figure 8(b) was scaled by the RMS coefficient ($\frac{1}{\sqrt{2}}$) for a sine wave. As shown in Figure 8(a), peak welder velocity changes linearly with amplitude setting while average weld power changes in a quadratic manner. Peak welder velocity is expected to change in a linear manner with applied voltage when no shear force is present, see (5). Likewise, voltage also changes linearly with the amplitude setting when there is no shear force present. Power, on the other hand is expected to change quadratically because it is a function of current squared when shear force is not present.

Because voltage and velocity are linearly related, the coupling constant for the mechanical mobility representation of the welder (Ψ_t) can be found by fitting a line between the two variables. As described in (6)-(8), Ψ_t is scaled by the mechanical admittance (H_m^*) to estimate H_{em}^*. As a result, applied peak current can be estimated by using Ψ_t, H_m^*, and measured peak welder velocity. Estimated peak current can then be used with measured RMS voltage to calculate average electric power, $P_{e,avg}$. Average electric power is defined as the multiplication

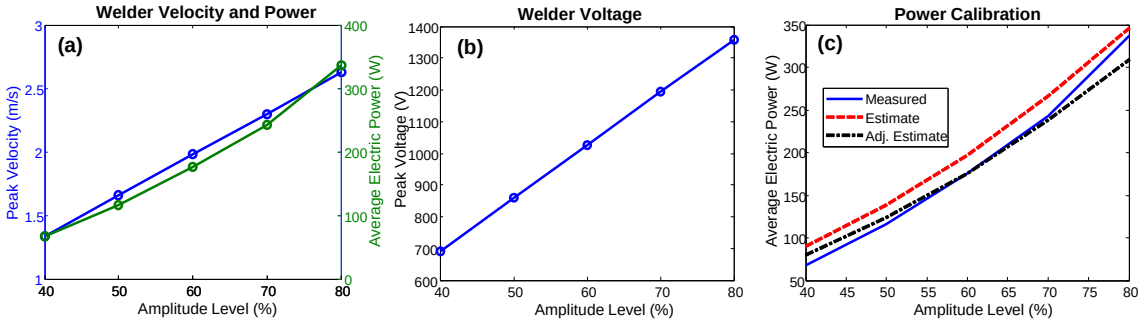

Figure 8. Operation of welder operating under no load, i.e., not welding: (a) comparison of peak welder velocity and average electric power draw as a function of amplitude setting; (b) applied voltage as a function of amplitude setting; (c) calibration of mechanical mobility model to average electric power.

of RMS voltage, RMS current, and the cosine of the phase angle (θ) between voltage and current,

$$P_{e,avg} = V_{RMS} i_{RMS} \cos\theta. \tag{11}$$

The H_e^* transfer function theoretically does not have a resonance and an anti-resonance due to the use of the motional feedback control strategy in UAM. Instead, the function will behave more like a single degree of freedom model and have a phase angle of zero at resonance, see (6). Thus, the phase angle between applied current and voltage can be assumed to be zero in the power expression (11). Using this phase angle simplification, the average electric power can be estimated and compared to the measurement, see Figure 8(c). The figure shows that the estimated power is higher than the measurement. To remedy this mismatch, the peak value of H_m^* was adjusted by increasing it 12%. The peak value of H_m^* was difficult to accurately measure during characterization, so increasing its value is likely more accurate as well. With this adjustment to H_m^*, the power estimate shows closer agreement with the measured value. The calculated constants utilized for this power calibration are listed in Table 2.

Model Variable	Value
Ψ_t (V*s/m)	515.3
Peak H_m^* (m/s/N)	0.010
Adjusted Peak H_m^* (m/s/N)	0.0112

Table 2. Coefficients used to validate mechanical mobility representation.

6. SHEAR FORCE ESTIMATION AND WELDER EFFICIENCY

It is shown in Figure 8(c) that power draw from the welder can be accurately estimated from the measured voltage, measured velocity, and estimated current when operating under no load, i.e., no welding. The expression for power (11) was computed assuming that the waveforms are sinusoidal or harmonic in behavior due to empirical observations of the voltage and velocity, see discussion in Section 5 and no welding trace in Figure 9, respectively. These signals also remain predominately sinusoidal during welding operations with some harmonic content in the velocity signal, see welding trace in Figure 9. This harmonic content is believed to originate from plastic deformation and slip during the process and not the electrical current excitation.[33] Because the 1^{st} harmonic of the welder velocity is an order of magnitude greater than all other higher order harmonics, it can be assumed that energy is concentrated at the excitation frequency. Consequently, the presented modeling framework at resonance (5) can be used to estimate current and resultant shear force with the use of measured average electric power.

The electrical current during welding can be estimated from welder power and the no welding reference state because applied voltage to the piezoelectric transducers is controlled to be constant for both the welding and no

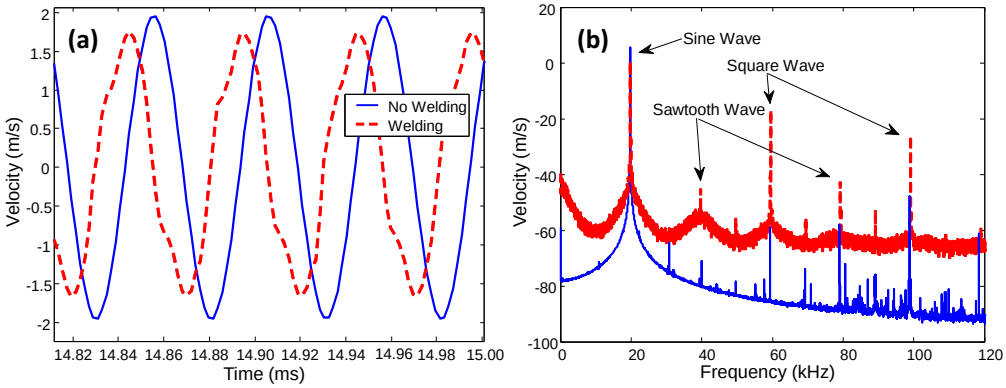

Figure 9. Sonotrode or welder velocity character during UAM compared to actuating the welder without load, i.e. not welding: (a) time history comparison of signals; (b) frequency domain comparison of signals. Signals were sampled at 512 kHz with an amplitude level of 60% (32.5 μm setpoint). The phase delay in (a) is of no significance. Frequency data was obtained by averaging the velocity signal magnitude with a block size of 81920 points and without windowing. Windowing was not used to illustrate increased frequency content more clearly. Due to windowing not being used, some leakage may be present in the figure.

welding states. Consequently, the ratio of average electric power between the two states can be be equated to the ratio of weld currents,

$$\frac{P_2}{P_1} = \frac{i_2}{i_1}, \tag{12}$$

where P_2 and P_1 are the average electric power for welding states 2 (welding) and 1 (no welding), respectively. Likewise, i_2 and i_1 are the applied peak electric current values for welding states 2 and 1. In section 5 the current was calibrated against measured average electric power for not welding (state 1) for multiple voltage values. The calibrated current can then be used to estimate current during welding with the use of expression (12) and measured power during welding. With this estimate for applied current, the welder shear force can then be estimated with the use of (5) and in-situ velocity,

$$F_s = \frac{H^*_{em} i - \dot{\delta}}{H^*_m}. \tag{13}$$

To illustrate the use of (13), the states of no welding and welding are compared, see Figure 10. Along with estimated shear force between the two states, the measured average electric power, measured peak welder velocity, and calculated excitation frequency are also shown in the figure. These other in-situ measurements were originally shown in Figure 3 at the onset of this paper. Signals were sampled at 50 kHz (25 kHz Nyquist) with a National Instruments DAQ module. Thus, content in Figure 10 is from the excitation signal (near 20 kHz) and contains no higher order harmonic content. The average electric weld power increases an order of magnitude, the welder excitation frequency increases 75 Hz, the peak welder velocity decreases 10%, and shear force is near 1750 N during welding. Similar force magnitudes were measured during the ultrasonic spot welding process for the same alloy processed under similar processing conditions.[39] The shear force on the welder exhibits similar behavior to the average electric power since (12) is used to estimate applied current to the welder. The reported average electric power in Figure 10 was measured from a single piezoelectric transducer and doubled in value because power draw is near symmetric between the two transducers.[37]

With the use of estimated peak shear force, measured peak welder velocity, and measured average electric power draw, welder efficiency (e) can then be calculated,

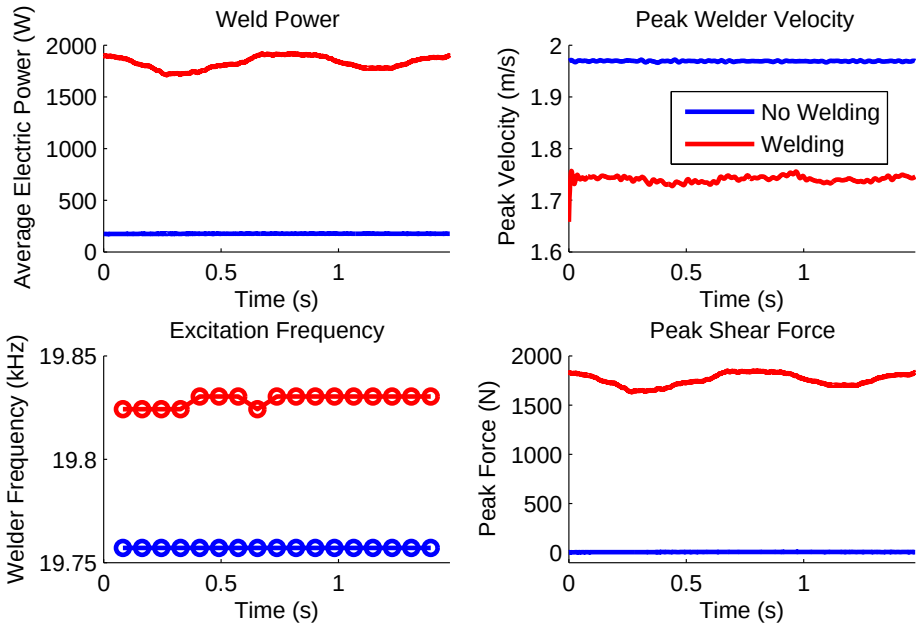

Figure 10. Estimate of welder shear force from in-situ velocity and power measurements. Welder excitation frequency is also compared to illustrate system stiffening when welding.

$$e = \frac{P_{m,avg}}{P_{e,avg}} = \frac{\frac{1}{2}\dot{\delta}F_s}{P_{e,avg}}. \tag{14}$$

Welder efficiency is calculated using the ratio of average mechanical power ($P_{m,avg}$) and average electric power ($P_{e,avg}$). This efficiency calculation assumes that the majority of the applied electrical energy is concentrated near the excitation frequency as well. Efficiency comparisons between the states of no welding and welding are shown in Table 3. The efficiency is not exactly zero when not welding because there is a small residual shear force from the calculation (13). Nontheless, the estimated welding efficiency is near estimates for ultrasonic metal welding systems[7] and below that of UAM piezoelectric transducers,[40] which is greater than 90%.

	No Welding	**Welding**
Mean	4.31	83.66
Std. Dev.	0.50	0.44

Table 3. Welder efficiency comparison between the states of not welding and welding. A small efficiency is calcualted for the state of not welding due to a small residual shear force being present from the calculation of shear force (13).

7. INFLUENCE OF UAM BUILD DYNAMICS

The influence of UAM build dynamics on system dynamics can be studied by replacing welder shear force in Figure 5(b) with a prescribed forcing function or a load impedance function (Z_{LD}) to describe energy transfer into the weld for UAM components. To describe UAM build dynamics in a general way for an Al 6061 stack, a complex stiffness[41] load impedance can be used,

$$Z_{LD} = \frac{k_{eff}}{j\omega}(1 + j\eta). \tag{15}$$

Where k_{eff} is the effective stiffness of the UAM build and η is the loss factor or energy transfer efficiency of the process. This complex stiffness expression describes UAM build stiffness and damping, independent of frequency. In other words, a hysteretic damping model was chosen to model system losses because plastic deformation character would show little change near the excitation frequency when the PLL controller moves the excitation frequency. Damping from plastic deformation is typically described with a Coulomb-friction model,[41] like bilinear hysteresis.[42,43] The purpose of the presented impedance function is not to describe the elasto-plastic interaction during UAM but to describe the UAM build dynamics in a general way.

To describe the influence of the UAM build onto the system, the load impedance was implemented by introducing effective build stiffness without damping initially ($\eta = 0$) and then introducing a loss factor ($\eta = 0.25$). To estimate the effective build stiffness, system stiffness was increased until a 75 Hz frequency shift was accomplished, see $\eta = 0$ traces in Figures 11-12. This 75 Hz frequency shift was chosen because it was observed when welding an Al 6061 stack, see Figure 3(b). The required build stiffness to cause this frequency shift is less than 1% of the assembly stiffness. Also, because energy is being stored in the system, no change in system response magnitude occurs. Because the welder is capable of moving the excitation frequency during welding, it can be inferred that FRF response will not change due to this added stiffness. For illustration purposes, a loss factor of 0.25 or a damping capacity of 25% was chosen to show the behavior of system losses during UAM due to large amounts of plastic deformation occurring. The $\eta = 0.25$ curves in Figures 11-12 illustrate that the system response decreases due to energy no longer being stored within the welding assembly and being transferred to the weld interface. A summary of key lumped parameter estimates for this analysis are shown in Table 4.

Model Variable	Value
K_t (GN/m)	30.49
k_{eff} (GN/m)	0.02
η	0.25

Table 4. Key lumped parameter values used to describe UAM stack dynamics. Effective build stiffness (k_{eff}) was chosen by increasing the system resonance 75 Hz. A high loss factor (η) was chosen to illustrate the influence of the large amount of plastic deformation on system response during UAM.

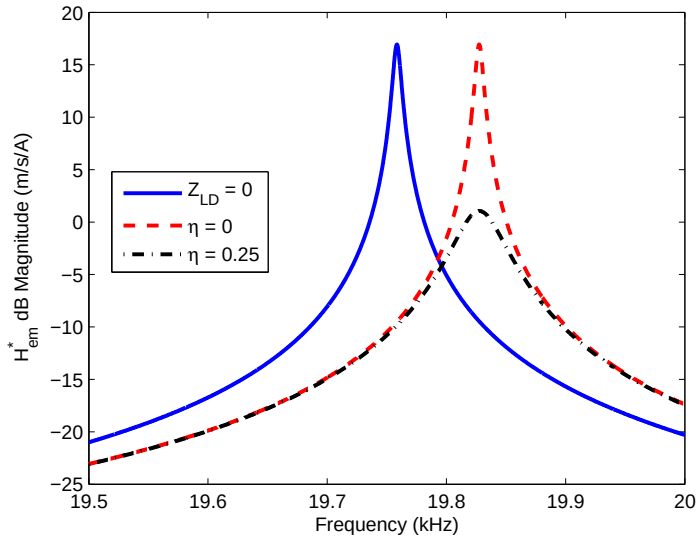

Figure 11. Estimation of UAM build stiffness via a 75 Hz frequency shift and the investigation of UAM build stiffness on FRF magnitude. Due to stiffness not influencing FRF magnitude, FRF magnitude would be consistent when system resonance changes under load. Damping or energy leaving the system is shown to decrease system response.

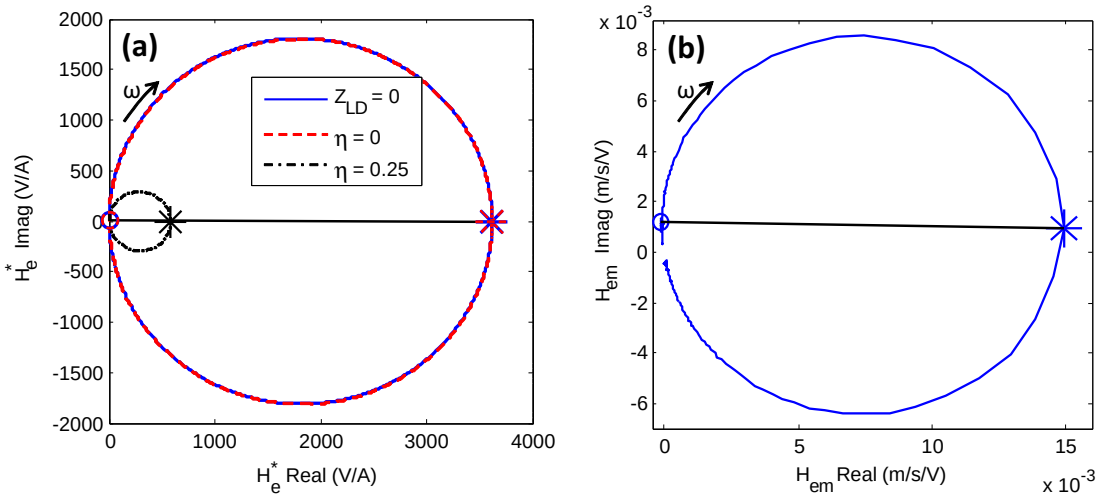

Figure 12. Nyquist plots: (a) estimated motional impedance locus, H_e^*; (b) measured admittance locus, H_{em}. Resonant frequencies for each locus are marked with an asterisk while adjacent locus points are marked with circles. Loading the system without damping does not change the motional impedance locus due to the diameter remaining constant. The decrease in locus diameter occurs only when damping is introduced.[35] The resonant frequency location in the motional impedance locus occurs at 0 degrees because the electro-mechanical coupling coefficient is assumed to be real valued.[35] To verify this assumption, the H_{em} admittance locus is plotted. The resonant peak has a phase location < 1 degrees, which supports the real valued coupling coefficient assumption of 0 degrees.

8. CONCLUDING REMARKS

A new linear time-invariant (LTI) model of the UAM process is proposed to describe process dynamics. In particular, the model explicitly specifies welder shear force as a system input to describe system dynamics compared to lumping the shear force or load into the dynamics of the welder. The modeled dynamics are a function of the piezoelectric transducers used to drive the system and the sonotrode. The welder was analyzed using equivalent circuit analysis, empirical FRF estimation, and characterization measurements. Using these measurements, LTI model parameters were found and assumptions verified. The Shear force load on the welder and welder efficiency were estimated using this model and in-situ measurements to be near 1750 N and 80%, respectively. Aside from estimating shear force, this LTI model can be used to study deformation behavior during the UAM process and the influence of changing process variables.

Acknowledgments

This material is based upon work supported by the National Science Foundation, CMMI Division Grant No. 1538275. Support for A.H. comes from a NSF Graduate Fellowship under Grant No. 1102690 and from the member organizations of the Smart Vehicle Concepts Center (www.SmartVehicleCenter.org), a National Science Foundation Industry/University Cooperative Research Center. Any opinions, findings, and conclusions or recommendations expressed in this material are those of the authors and do not necessarily reflect the views of the National Science Foundation. The authors would like to thank Prof. I.V. Adamovich and B. Goldberg of OSU's Non-Equilibrium Thermodynamics Laboratory for helping with the high voltage measurements of the welder.

REFERENCES

[1] White, D., "Ultrasonic consolidation of aluminum tooling," *Advanced materials & processes* **161**(1), 64–65 (2003).

[2] Graff, K., [*ASM Handbook: Volume 6A: Welding Fundamentals and Processes: Ultrasonic Additive Manufacturing*], American Society for Metals International (2011).

[3] Graff, K., Short, M., and Norfolk, M., "Very High Power Ultrasonic Additive Manufacturing (VHP UAM)," in [*International Solid Freeform Fabrication Symposium*], (2011).
[4] Wolcott, P., Hehr, A., and Dapino, M., "Optimized welding parameters for Al 6061 ultrasonic additive manufactured structures," *Journal of Materials Research* **29**(17) (2014).
[5] Neppiras, E., "Ultrasonic welding of metals," *Ultrasonics* **3**(3) (1965).
[6] Daniels, H., "Ultrasonic welding of metals," *Ultrasonics* **3**(4) (1965).
[7] Graff, K., [*AWS Handbook 9th Edition: Volume3: Ultrasonic Welding of Metals*], American Welding Society (2001).
[8] Johnson, K., *Interlaminar Subgrain Refinement in Ultrasonic Consolidation*, PhD thesis, Loughborough University, Loughborough, UK (2008).
[9] Dehoff, R. and Babu, S., "Characterization of interfacial microstructures in 3003 aluminum alloy blocks fabricated by ultrasonic additive manufacturing," *Acta Materialia* , 1–12 (March 2010).
[10] Sriraman, M., Babu, S., and Short, M., "Bonding characteristics during very high power ultrasonic additive manufacturing copper," *Scripta Materialia* **62**, 560–563 (January 2010).
[11] Fujii, H., Sriraman, M., and Babu, S., "Quantitative evaluation of bulk and interface microstructures in Al-3003 alloy builds made by very high power ultrasonic additive manufacturing," *Metallurgical and Materials Transactions A: Physical Metallurgy and Materials Science* **42**, 4045–4055 (December 2011).
[12] Sriraman, M., Gonser, M., Fujii, H., Babu, S., and Bloss, M., "Thermal transients during processing of materials by very high power ultrasonic additive manufacturing," *Journal of Materials Processing Technology* **211**, 1650–1657 (2011).
[13] Janaki Ram, G., Robinson, C., Yang, Y., and Stucker, B., "Use of ultrasonic consolidation for fabrication of multi-material structures," *Rapid Prototyping Journal* **13**(4), 226–235 (2007).
[14] Obielodan, J., Ceylan, A., Murr, L., and Stucker, B., "Multi-material bonding in ultrasonic consolidation," *Rapid Prototyping Journal* **13**(3), 180–188 (2010).
[15] Hopkins, C., Fernandez, S., and Dapino, M., "Statistical Characterization of Ultrasonic Additive Manufacturing Ti/Al Composites," *Journal of Engineering Materials and Technology* **132** (2010).
[16] Truog, A., *Bond Improvement of Al/Cu Joints Created by Very High Power Ultrasonic Additive Manufacturing*, Master's thesis, The Ohio State University, Columbus,OH (2012).
[17] Sietins, J. M., *Exploring Diffusion of Ultrasonically Consolidated Aluminum and Copper Films Through Scanning and Transmission Electron Microscopy*, PhD thesis, University of Delaware, Newark, DE, USA (2014).
[18] Kong, C., Soar, R., and Dickens, P., "Ultrasonic consolidation for embedding sma fibres within aluminium matrices," *Composite Structures* **66**, 421–427 (2004).
[19] Kong, C. and Soar, R., "Method for embedding optical fibers in an aluminum matrix by ultrasonic consolidation," *Applied Optics* **44**(30), 6325–6333 (2005).
[20] Siggard, E., *Investigative research into the structural embedding of electrical and mechanical systems using ultrasonic consolidation*, Master's thesis, Utah State University, Logan, UT (2007).
[21] Cheng, X., Datta, A., Choi, H., Zhang, X., and Li, X., "Study on Embedding and Integration of Microsensors Into Metal Structures for Manufacturing Applications," *Journal of Manufacturing Science and Engineering* **129**, 416–424 (2007).
[22] Hahnlen, R., *Characterization and Modeling of Active Metal-Matrix Composites with Embedded Shape Memory Alloys*, PhD thesis, The Ohio State University, Columbus, OH (2012).
[23] van der Burgt, C. and Pijls, H., "Motional Positive Feedback Systems for Ultrasonic Power Generators," *IEEE Transactions on Ultrasonics Engineering* **10**(1) (1963).
[24] Richter, B., Twiefel, J., and Wallaschek, J., [*Energy Harvesting Technologies: Ch4: Piezolectric Equivalent Circuit Models*], Springer (2009).
[25] Gibert, J. M., Austin, E. M., and Fadel, G., "Effect of height to width ratio on the dynamics of ultrasonic consolidation," *Rapid Prototyping Journal* **16**(4).
[26] Gibert, J. M., Fadel, G., and Daqaq, M. E., "On the stick-slip dynamics in ultrasonic additive manufacturing," *Journal of Sound and Vibration* **332**, 4680–4695 (2013).

[27] Robinson, C., Zhang, C., Janaki-Ram, G., Siggard, E., Stucker, B., and Li, L., "Maximum height to width ratio of free-standing structures built by ultrasonic consolidation," in [*Proceedings of the 17th Solid Freeform Fabrication Symposium*], (August 2006).
[28] Hehr, A., Wolcott, P. J., and Dapino, M. J., "Effect of Weld Power and Build Compliance on Ultrasonic Consolidation," *Rapid Prototyping Journal* **In Press**.
[29] Gibert, J. M., *Dynamics of Ultrasonic Consolidation*, PhD thesis, Clemson University, Clemson, SC, USA (2009).
[30] Graff, K., [*Power Ultrasonics: Ch6: Power ultrasonic transducers: principles and design*], Elsevier (2015).
[31] Neppiras, E., "New Magnetostrictive Materials and Transducers: Part I," *Journal of Sound and Vibration* **8**(3) (1968).
[32] Neppiras, E. A., "Motional feed-back systems for ultrasonic transducers," in [*Ultrasonics*], (1971).
[33] Hehr, A. and Dapino, M. J., "Dynamics of Ultrasonic Additive Manufacturing," *Ultrasonics* (In Review).
[34] "Dukane Communication." private communication (2015).
[35] Hunt, F., [*Electroacoustics: The Analysis of Transduction and Its Historical Backaground*], Cambridge: Harvard University Press (1954).
[36] Mason, W. P., [*Electromechanical Transducers and Wave Filters*], D. Van Nostrand Company, Inc. (1942).
[37] Hehr, A. J., *Process Control and Development for Ultrasonic Additive Manufacturing with Embedded Fibers*, PhD thesis, The Ohio State University, Columbus, OH, USA (2016).
[38] AE Techron, "Technical Manual: LVC5050 Power Supply Amplifier," (2002).
[39] de Vries, E., *Mechanics and Mechanisms of Ultrasonic Metal Welding*, PhD thesis, The Ohio State University, Columbus, OH, USA (2004).
[40] Friel, R., [*Power Ultrasonics: Ch13: Power ultrasonics for additive manufacturing and consolidation of materials*], Elsevier (2015).
[41] de Silva, C., [*Vibration: Fundamentals and Practice*], CRC Press LLC (2000).
[42] Caughey, T. K., "Sinusoidal Excitation of a System With Bilinear Hysteresis," *Journal of Applied Mechanics* **27**(4) (1960).
[43] Iwan, W., "A Distributed-Element Model for Hysteresis and Its Steady-State Dynamic Response," *Journal of Applied Mechanics* **33**(4) (1966).